ADVANCED MATERIALS INTERFACES
www.advmatinterfaces.de

# Rational Design of Transparent Nanowire Architectures with Tunable Geometries for Preventing Marine Fouling

*Jing Wang, Sudarat Lee, Ashley R. Bielinski, Kevin A. Meyer, Abhishek Dhyani, Alondra M. Ortiz-Ortiz, Anish Tuteja,* and Neil P. Dasgupta**

**Marine biofouling is a sticky global problem that hinders maritime industries. Various microscale surface structures inspired by marine biological species have been explored for their anti-fouling properties. However, systematic studies of anti-marine-fouling performance on surface architectures with characteristic length-scales spanning from below 100 nm to greater than 10 µm are generally lacking. Herein, a study on the rational design and fabrication of $ZnO/Al_2O_3$ core–shell nanowire architectures with tunable geometries (length, spacing, and branching) and surface chemistry is presented. The ability of the nanowires to significantly delay or prevent marine biofouling is demonstrated. Compared to planar surfaces, hydrophilic nanowires can reduce fouling coverage by up to ≈60% after 20 days. The fouling reduction mechanism is mainly due to two geometric effects: reduced effective settlement area and mechanical cell penetration. Additionally, superhydrophobic nanowires can completely prevent marine biofouling for up to 22 days. The nanowire surfaces are transparent across the visible spectrum, making them applicable to windows and oceanographic sensors. Through the rational control of surface nano-architectures, the coupled relationships between wettability, transparency, and anti-biofouling performance are identified. It is envisioned that the insights gained from the work can be used to systematically design surfaces that reduce marine biofouling in various industrial settings.**

## 1. Introduction

Marine biofouling is a sticky global problem due to the vast diversity of fouling organisms and adhesion mechanisms that hinder a range of maritime applications.[1] Issues associated with marine biofouling include increased fuel consumption from drag,[2] safety concerns from corrosion,[3] and attenuation of sensor signals.[4] Challenges specific to the marine environment include development of robust fouling solutions for a diverse range of biological species and local ocean conditions, toxicity associated with commercial anti-fouling paints, and manufacturing challenges associated with coating a range of materials and non-planar geometries. For example, to prevent fouling on windows and other viewing surfaces, it is critical to maintain optical transparency. This prevents the potential use of common anti-fouling paints.[5]

To overcome these challenges, surface micro/nanostructures have attracted significant recent attention. This is in part because numerous marine species (e.g., shark skin,[6] crab eyes,[7] seashell[8]) have evolved to adopt surface micro/nanostructures to prevent marine fouling.[9] Inspired by these marine species, a range of structures with characteristic length-scales typically ranging from micrometers to millimeters have been designed and fabricated to reduce marine fouling.[10] Such surfaces have been tested within both single-species (e.g., *Ulva* spores, marine diatoms, barnacle larva)[10b,d] and multi-species (e.g., field tests in the ocean)[10a] environments. However, most

Dr. J. Wang, Dr. S. Lee, Dr. A. R. Bielinski, A. M. Ortiz-Ortiz, Prof. N. P. Dasgupta
Department of Mechanical Engineering
University of Michigan
Ann Arbor, MI 48109, USA
E-mail: ndasgupt@umich.edu
Dr. K. A. Meyer
School for Environment and Sustainability
University of Michigan
Ann Arbor, MI 48109, USA
A. Dhyani, Prof. A. Tuteja
Department of Macromolecular Science and Engineering
University of Michigan
Ann Arbor, MI 48109, USA
E-mail: atuteja@umich.edu
The ORCID identification number(s) for the author(s) of this article can be found under https://doi.org/10.1002/admi.202000672.
A. Dhyani, Prof. A. Tuteja
Biointerfaces Institute
University of Michigan
Ann Arbor, MI 48109, USA
Prof. A. Tuteja
Department of Materials Science and Engineering
University of Michigan
Ann Arbor, MI 48109, USA
Prof. A. Tuteja
Department of Chemical Engineering
University of Michigan
Ann Arbor, MI 48109, USA

**DOI: 10.1002/admi.202000672**

 

of the surface microstructures studied to date have focused on reducing fouling of a single species; in contrast, surface structuring has often demonstrated minimal reduction, or even an increase in fouling when exposed to a multi-species environment.[10a,b]

Additionally, nanoscale surface structures (ranging from <100 nm to hundreds of nanometers) have been explored for their antibacterial properties in biomedical applications.[11] However, nanoscale surface architectures with tunable geometric control have not yet been systematical studied in marine fouling environments. It has been widely reported that marine biofouling follows a linear "successional" model[1,12] in which smaller species (cyanobacteria, etc.) settle and grow first, followed by spores of macroalgae (diatoms, etc.) within the first week, and finally within several weeks, by larvae of invertebrates (barnacles, etc.). Accordingly, we hypothesize that nanoscale structures can be used to impact the initial settlement and growth of marine cyanobacteria, and further prevent or delay subsequent fouling based on the "successional" model.[1,12] In general, systematic studies of marine biofouling on surface architectures with characteristic length-scales that span a range from below 100 nm to above 10 μm could lead to new mechanistic insight into the development of anti-marine-fouling coatings, but are lacking.

One of the major challenges associated with systematically studying marine fouling on surface textures at these extremely small length-scales is the availability of scalable nano-fabrication processes that enable systematic tuning of feature geometries on a variety of non-planar substrates. Most current fabrication methods to create controlled nanoscale architectures depend on different patterning processes (e.g., lithography), which are restricted in their substrate compatibility, scalability, and cost.[11a,13] In addition, it is challenging to apply lithography techniques to fabricate nanostructures on complex geometries, such as curved surfaces and fabrics. Alternative patterning and deposition methods (e.g., self-assembly) can provide precise control over periodic geometries.[14] However, the ability to decouple independent geometric parameters in 3D (width, spacing, aspect ratio), which maintain conformal coverage over large areas and on non-planar surfaces, is a challenge for many of these techniques.

Herein, we present a study on the rational design and systematic control of nanowire (NW) architectures with tunable geometric parameters (length, spacing, and branching), using atomic layer deposition (ALD) for surface-directed nucleation and growth of hydrothermal NWs.[15] We have previously demonstrated that this approach allows for the systematic fabrication of NW architectures independent of the underlying surface geometry or composition, and can be used to tune surface wetting to enable superomniphobic surfaces by design.[15a]

In this study, the effect of surface chemistry and geometry on marine algal fouling in a multi-species environment is systematically studied for core–shell, or core–shell–shell, NW structures. It is shown that unfunctionalized NW structures can delay algal biofouling for ≈15 days, and reduce the surface coverage of fouling by up to ≈60% after 20 days compared to the untreated surfaces, while maintaining optical transparency. The mechanism of fouling reduction on the hydrophilic NWs can be attributed to two effects: 1) the NWs reduce the effective contact area with the fouling marine algae due to a steric hindrance to cell settlement; and 2) NWs produce a mechanical biocidal effect on the settled algae. The impact of NW geometry (length, spacing, and branching) on these effects was studied by systematic tuning the surface architecture.

Additionally, superhydrophobic NWs surfaces, fabricated by functionalizing the produced NWs with a low-surface-energy silane, demonstrated complete fouling prevention for ≈20 days and reduced the fouling coverage for more than 50 days. The durability of the superhydrophobicity obtained on different NW architectures can be explained through thermodynamic and mass transfer analysis and helps provide design principles for fabricating superhydrophobic anti-fouling coatings. In addition, the NW architectures were all transparent across the visible spectrum, demonstrating their feasibility on windows and optical surfaces. Overall, our work systematically discusses and demonstrates the design of anti-biofouling NW architectures with length-scales spanning from below 100 nm to greater than 10 μm. By decoupling the impacts of NW geometry and surface chemistry, this study provides new insights into the rational design of anti-marine-fouling coatings at the nanoscale.

## 2. Results and Discussion

### 2.1. Fabrication of NW Surfaces

Marine algae are a complex mixture of diverse species with a characteristic size range from sub-micron to tens of micrometers (Figure S1, Supporting Information). Therefore, to study the impacts on marine fouling of surface textures that span these length-scales, ZnO NW arrays with tunable length, spacing, and branching were prepared using a previously published method of surface-directed assembly that combines ALD with hydrothermal NW growth[15] (see details in Experimental Section). Specifically, shown in **Figure 1**a and Figure S2, Supporting Information, the substrate (e.g., glass) was coated with a 20 nm seed layer of ALD ZnO, followed by a sub-monolayer "overlayer" of ALD $TiO_2$. By controlling the number of ALD $TiO_2$ cycles in this overlayer, the nucleation density of ZnO NWs can be monotonically tuned during subsequent hydrothermal growth with controlled inter-NW spacing from ≈40 nm to >10 μm.[15a] As shown by scanning electron microscope (SEM) analysis, the length of the NWs was tuned by varying the hydrothermal growth time (Figure 1b), while the spacing of the NWs was tuned by increasing with the number of ALD $TiO_2$ overlayer cycles (Figure 1c). In addition to controlling NW length and spacing, branched NWs (BNWs) with controlled spacing were fabricated by a multi-step ALD-seeding/hydrothermal growth process (Figure 1d; Figure S2b, Supporting Information).[15a] Figure 1 shows a series of SEM images of the resulting NW and BNW morphologies to demonstrate the tunable control of the NW architecture. After the hydrothermal growth, the NWs were subsequently coated with a 5 nm $Al_2O_3$ shell to form a core–shell structure (Figure S2c, Supporting Information). This shell served to prevent ZnO dissolution in the aqueous environment and enabled subsequent surface functionalization (further details in Experimental Section). Furthermore, the NWs can withstand normal shear flow (Figures S3 and S4, and Table S1, Supporting Information) and strong fluid and acoustic cleaning

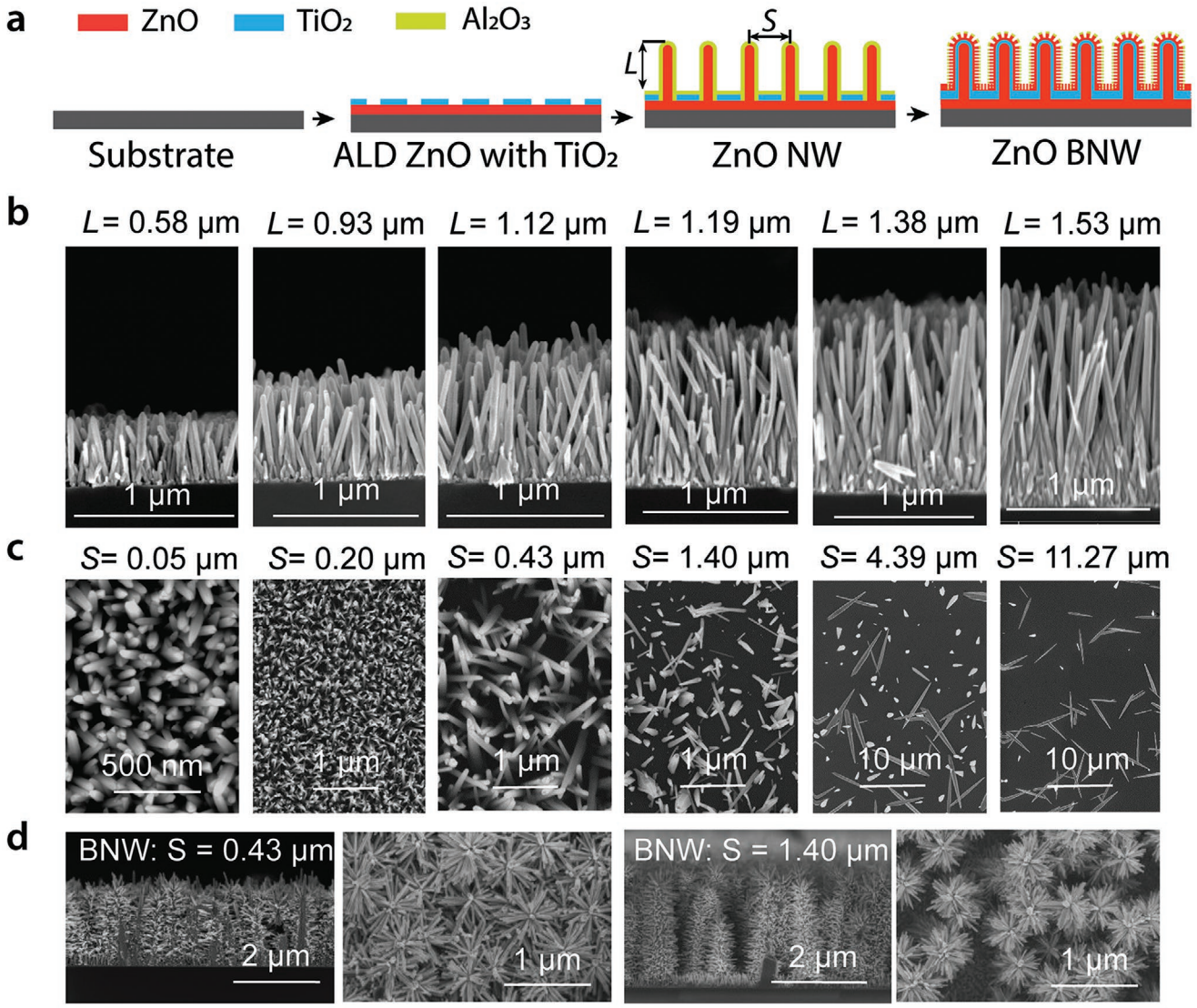


**Figure 1.** Fabrication of NWs with tunable geometries. a) A schematic illustrating the NW fabrication process. b) SEM images of NWs with different lengths ($L$) ranging from 0.58 to 1.53 μm fabricated using different hydrothermal growth time from 15 to 105 min. These NWs have similar inter-NW spacing as ≈0.05 μm. c) SEM images of NWs with different inter-NW spacing ($S$) ranging from 0.05 to 11.37 μm. These NWs have similar NW length as ≈1.50 μm. The inter-NW spacing was modulated by changing the number of ALD $TiO_2$ cycles from 0 to 7 cycles. d) BNWs with varying spacing between the base NWs.

process (Figure S5, Supporting Information). Moreover, we demonstrated that this fabrication method can be applied to larger length scales and to non-planar surfaces (Figure S6 and Video S1, Supporting Information).

### 2.2. Optical Transparency Characterization

The optical transparency of the NW architectures was characterized using UV–vis spectrophotometry. As shown in **Figure 2**, all of the NW geometries were transparent across the visible spectrum, with an absorption onset in the UV region that corresponds to the bandgap of ZnO. For all high-density NWs (inter-NW spacing $S < 100$ nm) the samples transmitted >90% of light at wavelengths above 500 nm, and >80% between 400 and 500 nm (Figure 2a,b). The transmittance decreased with increasing inter-NW spacing, which can be attributed to diffused light scattering that results from a slight decrease in NW angle with respect to the substrate normal (Figure 1c). Following this trend, the BNWs have a transmittance greater than 60%, which is attributed to increased scattering from the branches. In addition to total transmittance, the haze for each sample was quantified to illustrate the optical clarity of the samples (Figure S7, Supporting Information).

### 2.3. Wettability Characterization

In order to decouple the roles of surface geometry and surface functionalization on marine fouling, we fabricated

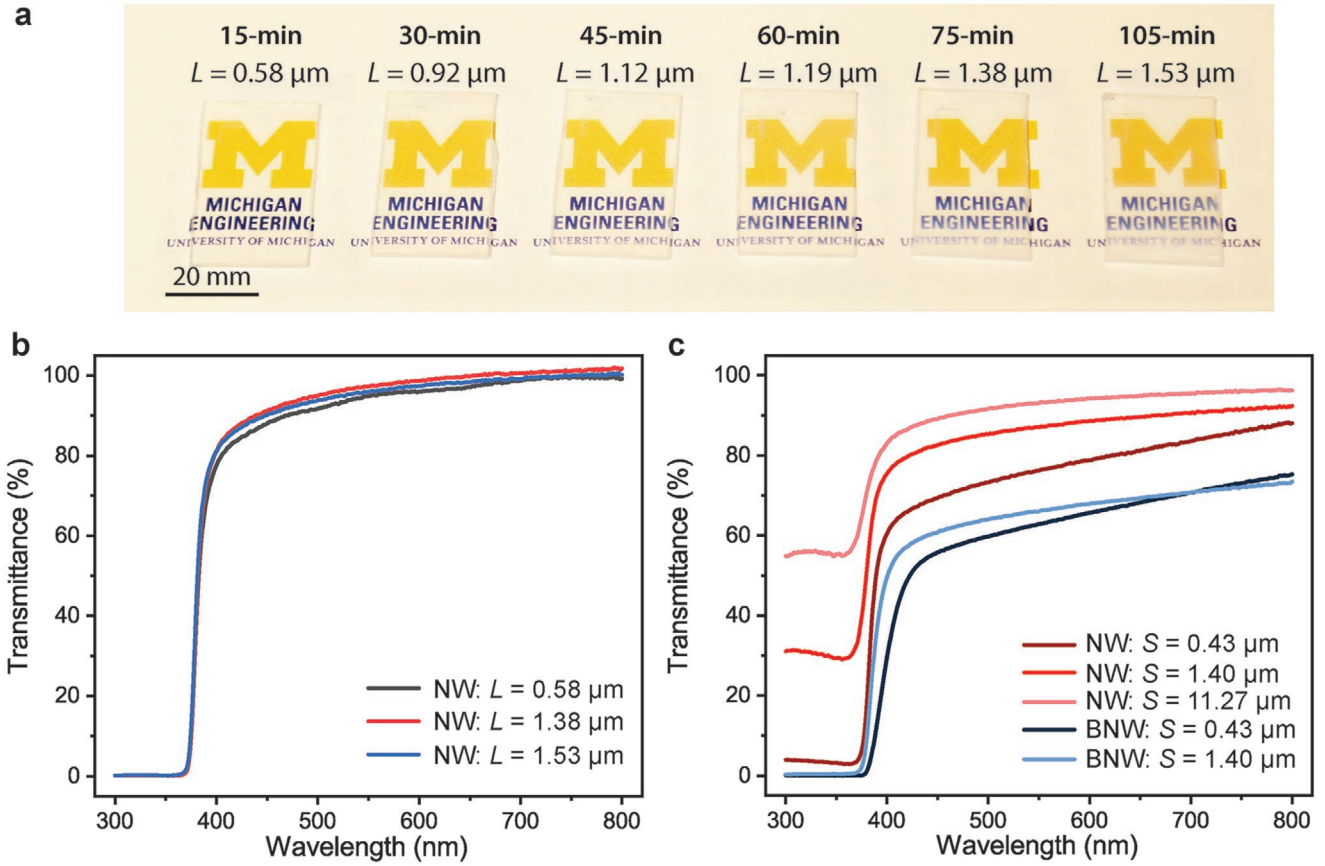


**Figure 2.** Optical characterization on the different NW surfaces fabricated on glass. a) Optical image demonstrating the transparency of the fabricated NW surfaces. b) Transmittance of NWs with different lengths and similar inter-NW spacing (≈0.05 μm). c) Transmittance of NWs with different inter-NW spacing and branching and similar NW length (≈1.50 μm).

both hydrophilic and superhydrophobic NWs (**Figure 3**a) with tunable geometries. The ALD $Al_2O_3$ shell on the NWs is intrinsically hydrophilic due to its high surface energy (≈900 mJ $m^{-2}$),[16] as confirmed by contact angle measurements (Figure 3b). Therefore, the wetted NWs in these hydrophilic samples were in the Wenzel state,[17] which fully exposed the NW surfaces to the marine environment.

In contrast, superhydrophobic NWs were fabricated by surface functionalization of the NWs with a perfluorinated silane (see in Experimental Section). The water repellency of the silanized NWs was confirmed through contact angle and contact angle hysteresis measurements (Figure 3). The silanized NWs possessing small inter-NW spacing (<100 nm) and varying lengths were all superhydrophobic (Figure 3b). The contact angle increased slightly with increasing NW length, which can be explained by a slight increase in inter-NW spacing at the tips with increasing length (Figure 1b). As the silanized NW spacing was increased to be above ≈3.2 μm, water wet the surface and entered the Wenzel state. This is because of the decrease in the breakthrough pressure, i.e., the applied pressure which forces the transition from the Cassie–Baxter state to the Wenzel state (see Figure 3a), with increasing NW spacing.[18] Furthermore, based on the modified Furmidge equation,[19] we can estimate the sliding angles from the advancing and receding angles of each surface (Tables S2 and S3, Supporting Information). All of the BNWs were superhydrophobic with low contact angle hysteresis (Table S4, Supporting Information). In addition, we demonstrated that the superhydrophobic NWs are stable under hydrostatic pressure with DI water (depth: 300 mm for 10 days) (Figure S8, Supporting Information), long exposure to seawater (1 month, Figure S9, Supporting Information) and ambient environment (>1 year, Table S5, Supporting Information).

### 2.4. Algal Fouling on Hydrophilic NWs

#### *2.4.1. Algal Fouling Performance*

We first studied the fouling of hydrophilic NWs (without silanization) as a function of geometry by submersing the samples in artificial seawater with 1 g wet biomass of algae. The marine algae in this study were originally collected from the coast of Florida (USA), and have been previously utilized to study marine biofouling.[2,20] The culture contains multiple species[2,21] including cyanobacteria and diatoms (Figure S1, Supporting Information). The sample area covered by fouling was imaged every day for 50 days using optical microscopy, and quantified using ImageJ analysis (see Experimental Section; Figure S10, Supporting Information). As seen in the optical microscopy images (**Figure 4**a and Supporting Information) of the surfaces

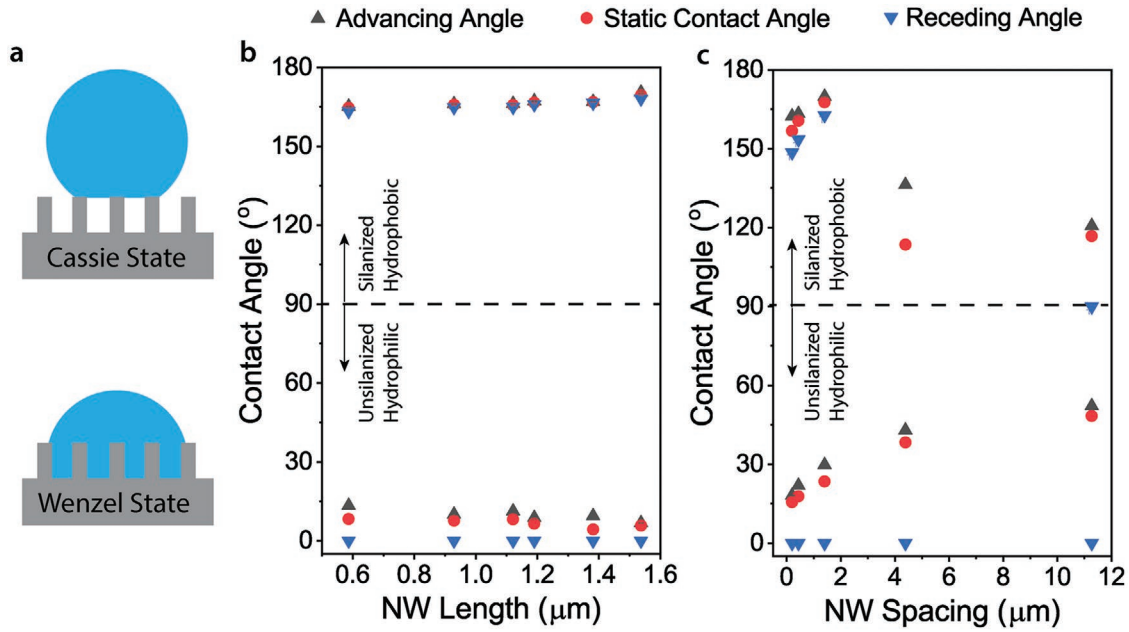


**Figure 3.** Contact angle measurement on hydrophobic NWs. a) Schematics illustrating Cassie–Baxter and Wenzel states. b) Contact angle and contact angle hysteresis measurements on unsilanized and silanized NWs with different lengths. c) Contact angle and contact angle hysteresis measurements on unsilanized and silanized NWs with different inter NW spacings. Error bars were obtained from at least five independent measurements.

after 20 days fouling, all of the NW surfaces showed significant fouling reduction compared to the planar control.

Specifically, the planar control with the same surface chemistry as the NWs (5 nm ALD-coated $Al_2O_3$) was completely covered by fouling after ≈20 days, while the hydrophilic NWs with different lengths and degrees of branching showed ≈50% less coverage within the same time period (Figure 4b,c). Approximately 35 days were required for the hydrophilic NWs to be 100% covered with a biofilm, representing a delay of ≈15 days compared to the control. From the data shown in Figure 4b,c, it is clear that the fouling rate on the hydrophilic samples was relatively independent of NW length and branching. In contrast, the fouling rate increased with increasing inter-NW spacing. From Figure 4d, the areal coverage was ≈50%, ≈65%, ≈75%, and ≈90% after 20 days on NWs with a spacing of 0.05 ± 0.01, 0.43 ± 0.17, 1.40 ± 0.49, and 11.27 ± 2.02 μm, respectively. To confirm that these trends were not a function of the algal concentration, we evaluated and observed the same relative fouling rates in an environment where the initial algae concentration was reduced by 50% (Figure S11, Supporting Information).

The fouling coverage area fraction is a 2D projection of a 3D biofilm structure. To confirm that this is an accurate representation of the total extent of marine biofouling, we performed optical density measurements[22] on the fabricated surfaces after 20 days of fouling. In these tests, a staining dye is absorbed by the cells, which is subsequently dissolved into dimethyl sulfoxide (DMSO). By measuring the optical absorbance of the dye solution, a quantitative measurement of the total volume of cells attached to the surface can be obtained. As shown in Figure S12, Supporting Information, the trends observed in the optical density measurements were in agreement with the areal coverage from optical microscopy, which indicates the uniformity of the biofilm across the fouled area on the surface, and further validates the use of the algae coverage area fraction as a quantitative measure of fouling extent.

### 2.4.2. Fouling Reduction Mechanism on Hydrophilic NWs

The fouling reduction on the hydrophilic NWs can be attributed to two main factors: 1) size-selective settlement of different marine species based on the inter-NW spacing; and 2) a mechanical biocidal effect arising from deformation of the settled bacteria on the NW surfaces.[11a,11b,23] Each of these mechanisms are discussed in further detail below.

*Size-Selective Settlement Mechanism*: The first mechanism for the reduced fouling rate arises from our ability to tune the NW geometry at the characteristic length scales that match the size of the various fouling marine species (e.g., cyanobacteria and diatoms). We observed the initial settlement of the marine algae on surfaces with different inter-NW spacings after 2 days of fouling. Cross-sectional SEM images (**Figure 5**a) demonstrate that the density of algae settlement between the NWs increased with increasing inter-NW spacing (further details in the Supporting Information). Specifically, when the inter-NW spacing was larger than ≈300 nm, bacteria were observed in the gaps between NWs. In contrast, for smaller inter-NW spacings, no settlement was observed between the NWs, and bacteria were only able to settle on the top surface of the NW array. We attribute this to steric hindrance, as the smallest length-scale of bacteria observed was ≈200 nm. Similarly, diatom settlement between the NWs was only observed when the inter-NW spacing was greater than 10 μm, which is the characteristic size of the diatoms observed in this study. Further statistical analysis of these trends at different locations along the surface is provided in the Supporting Information (Figure S13, Supporting

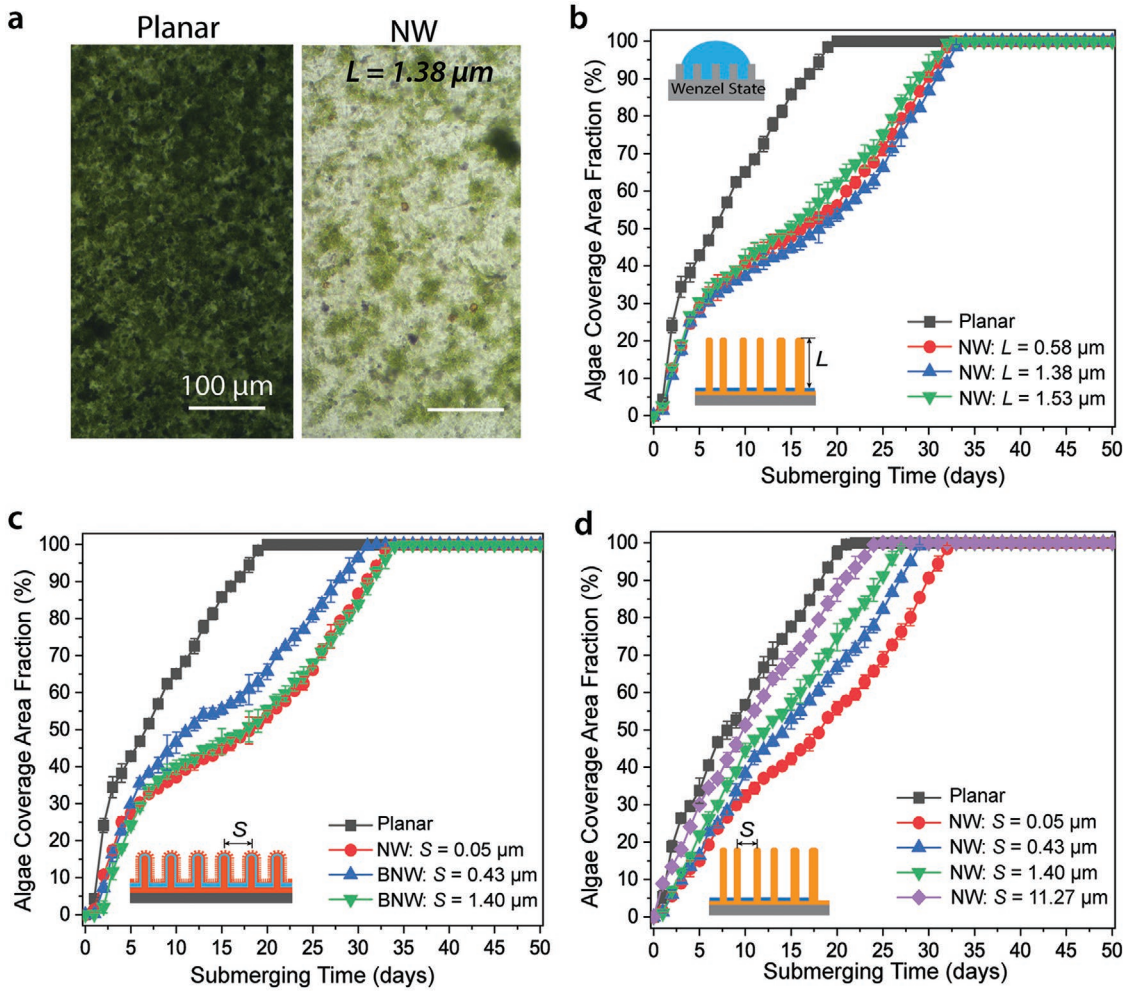


**Figure 4.** Marine algae fouling on different hydrophilic NW surfaces. a) Optical microscopy images comparing hydrophilic NW and planar control surfaces after 20 days of algal fouling. b) Algae coverage area fraction on NWs with different lengths and similar spacing (≈0.05 μm) in the Wenzel state for 50 days. c) Algae coverage area fraction on BNWs in the Wenzel state for 50 days. d) Algae coverage area fraction on NWs with different inter-NW spacings and similar length (≈1.50 μm) in the Wenzel state for 50 days. Errors bars were obtained from at least three independent measurements.

Information). These trends illustrate that the fouling species are able to access a larger fraction of the surface area for settlement as the inter-NW spacing increases (Figure 5b).

To reconcile these initial settlement observations with the fouling coverage area fraction results after extended time (shown in Figure 4d), we propose the following mechanism. When the inter-NW spacing is smaller than the characteristic length scale of bacteria, the rate of settlement between the NWs is very small, and therefore, the settlement focuses at the top surfaces of the NWs. This represents a smaller effective surface area than a planar sample, since the contact points are only at the tips of the NW. As discussed in the second mechanism below, this tip-contact with the cells also leads to a mechanical bactericidal effect.

As the inter-NW spacing increases within the range of 300 nm–10 μm, the accessible surface for settlement increases, and bacteria are able to grow within the inter-NW voids. This mechanism increases the fouling rate as the inter-NW spacing increases. Eventually, as the inter-NW spacing continues to increase, a larger fraction of the underlying planar surface is available for settlement. The planar surface facilitates settlement of a more diverse range of species, including diatoms. These trends indicate that the modulation of initial settlement can have a strong impact on the longer-term bio-fouling growth rate, as shown in Figure 5c.

*Mechanical Biocidal Effect*: The second mechanism for reducing the fouling rate on the NW surfaces relates to the biocidal effect that arises from mechanical interactions between the NWs and bacteria. This effect is known within the natural world; for example, dragonfly/cicada wings have strong bactericidal properties that arise from their nanostructured surfaces.[11a,d] These effects have been shown to be independent of surface chemical composition, and arise from the surface texture, rather than material toxicity.

To demonstrate that our NW arrays possess similar biocidal properties, we analyzed the surfaces after 5 days of fouling test through fluorescent microscopic imaging using LIVE/DEAD bacteria stains.[24] In **Figure 6**a, we observe an increased

 

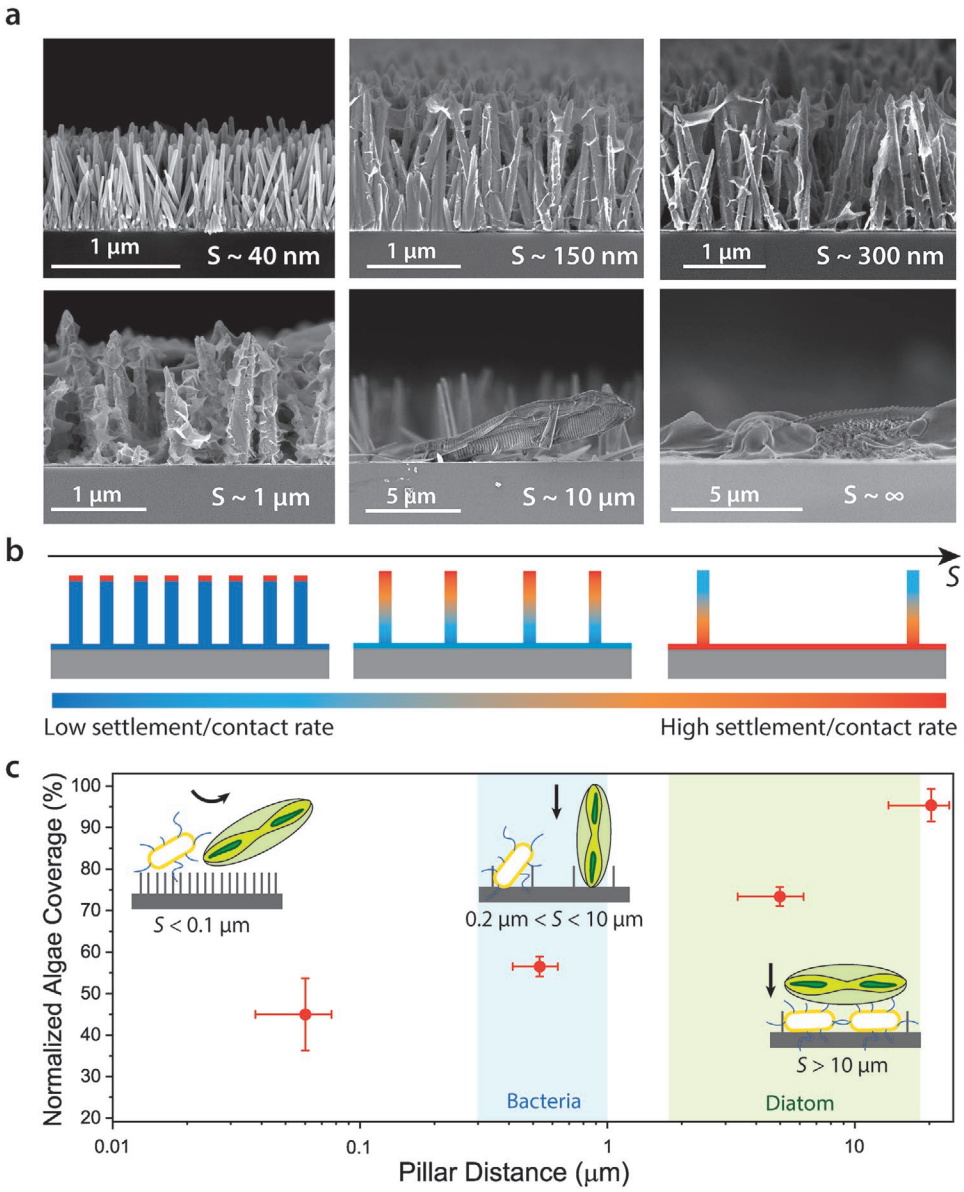


**Figure 5.** Size-selective settlement mechanism for fouling reduction on hydrophilic NWs. a) Cross-sectional SEM images of NWs with different spacing after 2 days of fouling. b) Schematic illustrating the spatial variation in fouling rate along the surface of NWs with different spacings. c) The algal fouling coverage area fraction, which has been normalized by the planar control on NWs with different spacings after 20 days. Errors bars were obtained from at least three independent measurements.

fluorescence signal from total-cell dye (fluorescent color: green) as inter-NW spacing increases. This is consistent with the trends shown in Figure 4d, wherein the fouling rate increases with increasing inter-NW spacing. Furthermore, we observed that the fraction of total cells that are dead (fluorescent color: red) decreases as inter-NW spacing increases. Similar trends are observed in the hydrophilic NW samples with different NW lengths and degrees of branching (Figures S14 and S15, Supporting Information). This indicates that as the inter-NW spacing decreases, a mechanical biocidal effect, similar to naturally nanostructured anti-bacterial surfaces, can be observed. This leads to the death of the initial bacteria that settle on the closely packed NW surfaces, and slows the subsequent bio-film growth kinetics.

To confirm that this biocidal effect is purely a geometric effect and not caused by Zn-ion dissolution into the aqueous solution, we performed inductively coupled plasma mass spectrometry (ICP-MS) measurements (Figure S17, Supporting Information). Owing to the presence of the $Al_2O_3$ shell on the NW surfaces, the concentration of Zn ions in the solution was found to be well below the toxicity level for marine algae.[25] Therefore, we conclude that it is the physical geometry, rather than the chemical composition of the NWs, that leads to their anti-bacterial properties.

These results on the mechanical toxicity of the fabricated NWs towards marine algae are consistent with previous studies on the anti-bacterial properties of other nanoscale

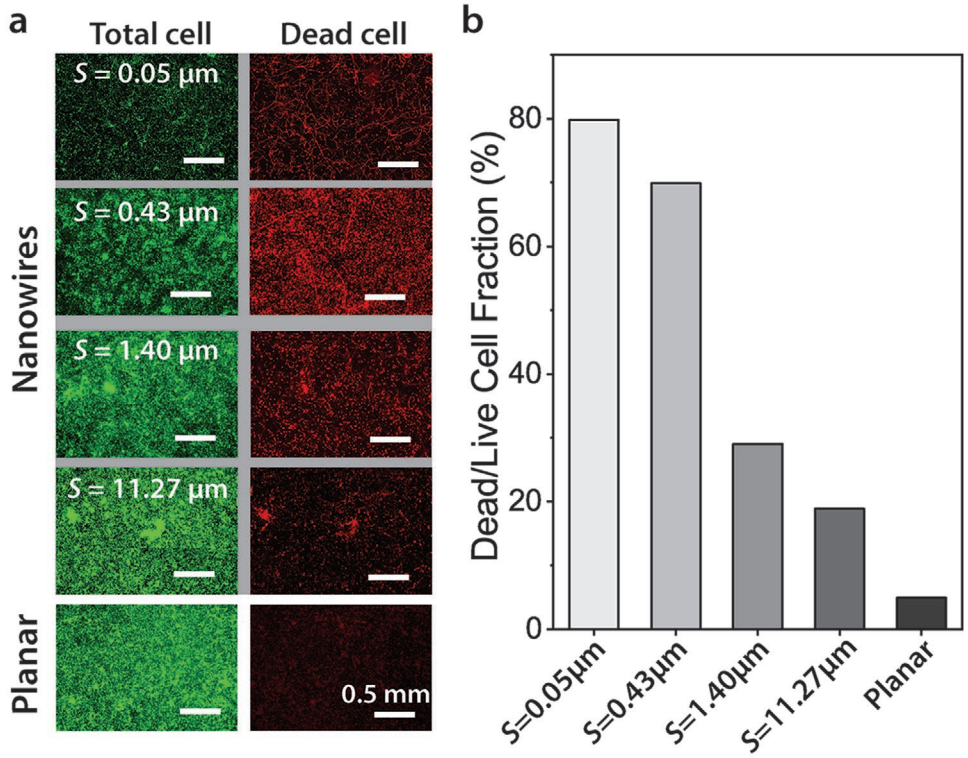


**Figure 6.** Mechanical biocidal effect of hydrophilic NWs. a) Fluorescent microscopic images of NWs with different inter-NW spacing after submerging in marine algae culture solution for 5 days. b) Dead cell percentage as a function of substrate geometry.

surface architectures (e.g., black silicon[11a] and graphite[26]). Mechanical biocidal effects have been attributed to multiple mechanisms, for example, mechanical penetration of the cells,[11a] destructive extraction,[27] and storage and release of mechanical energy.[11b] While a full mechanistic understanding of these coupled mechanical-biocidal effect requires further investigation, it is clear that the rational design of hydrophilic NW architectures can be used to tune size-selective settlement and mechanical interactions during the initial settlement, which can both contribute to improved anti-fouling performance.

### 2.5. Algal Fouling on Superhydrophobic NWs

#### *2.5.1. Algal Fouling Performance*

To study the effect of surface wettability on marine fouling, superhydrophobic NWs were functionalized via reaction with a low-surface-energy fluoro-silane, and tested under the same marine environment (**Figure 7**a and Supporting Information). For high-density superhydrophobic NWs with varying lengths, fouling was completely prevented for 7–12 days, and the time to reach 100% area coverage was 28–35 days longer than the planar control with the same surface chemistry (i.e., functionalized with fluoro-silane) (see Figure 7b). An increase in the length of the NWs resulted in a monotonic increase in the duration of the Cassie–Baxter state underwater, as shown by the increased residence time before the onset of fouling.

Furthermore, unlike the BNWs in Wenzel state (Figure 4c), the BNWs in the Cassie–Baxter state exhibited an increased duration in fouling prevention compared to unbranched NWs (Figure 7c). Specifically, the BNWs remained unfouled for 17–22 days, a period of greater than 50 days transpired before full algal areal coverage was observed on these surfaces (see in Figure 7c).

The fouling performance of the hydrophobic NWs was also observed to vary with the inter-NW spacing. Since NWs with a spacing of 11.27 ± 2.02 μm were in Wenzel state even after silanization (Figure 3b), their fouling performance was similar to the unsilanized (hydrophilic) surfaces with large inter-NW spacing. This indicates changing surface chemistry alone does not have a strong effect on the NW's anti-fouling properties when wetting occurs. Similarly, the algal fouling coverage was close to the planar control (Figures 4d and 7d) when the inter-NW spacing was greater than 10 μm.

In contrast, when the inter-NW spacing was small enough to maintain the Cassie–Baxter state, a minimum in surface fouling as a function of NW spacing was observed. Specifically, the NWs with an intermediate spacing of $S = 0.43 \pm 0.17$ μm outperformed the NWs with smaller ($S = 0.04 \pm 0.01$ μm) and larger ($S = 1.40 \pm 0.49$ μm) spacing. The NWs with a spacing of 0.43 μm were completely unfouled for more than 20 days, and increased the time required to reach 100% areal fouling coverage by >50 days when compared to the planar control (Figure 7d). As with the hydrophilic samples, we performed optical density measurements on the hydrophobic surfaces, and the results were found to be consistent with the trends observed in the 2D areal coverage data (Figure S12, Supporting Information).

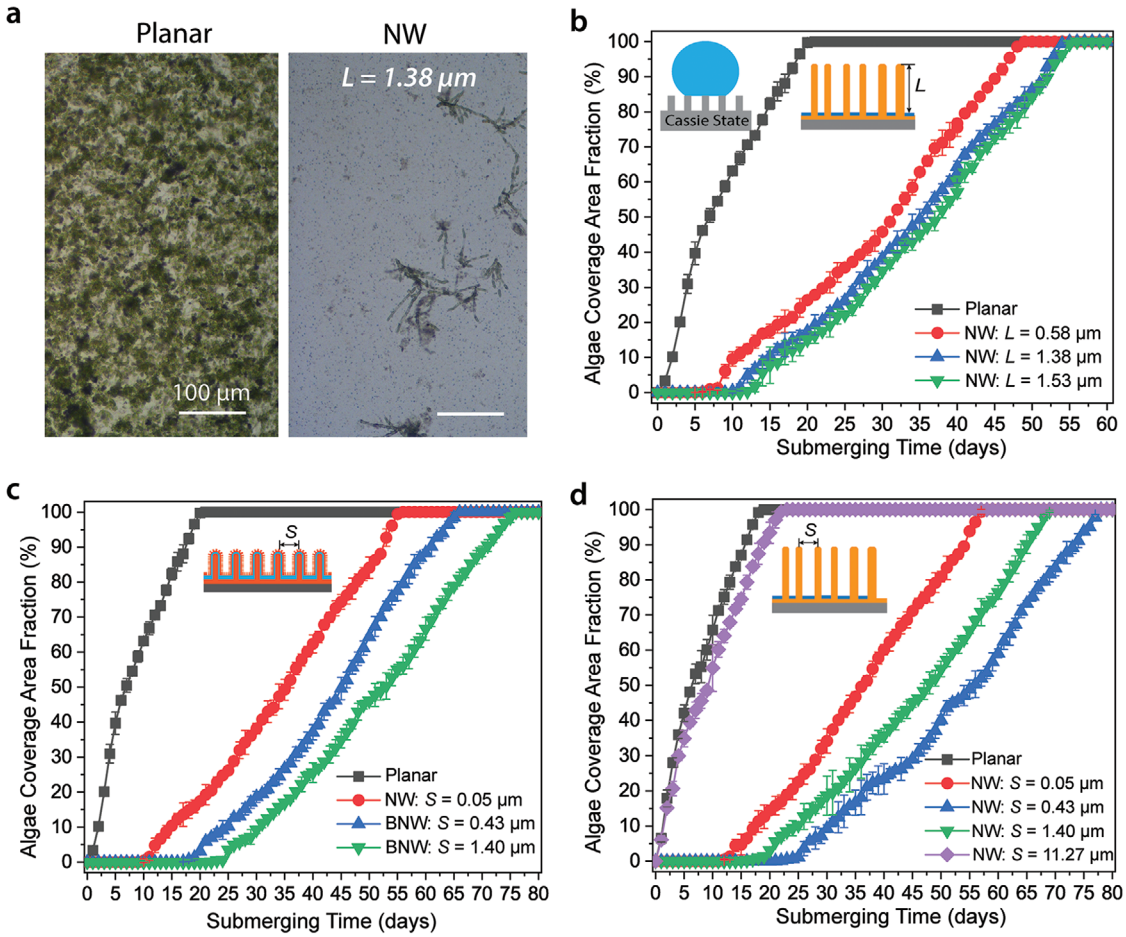


**Figure 7.** Marine algae fouling coverage on superhydrophobic NWs surfaces. a) Optical microscopy images for planar and NW surfaces after 20 days of algae fouling. b) Algae coverage area fraction on high-density NWs as a function of NW length for 60 days. The inter-NW spacing of these NWs was ≈0.05 μm. c) Algae coverage area fraction on BNWs for 80 days. d) Algae coverage area on NWs with different inter-NW spacings and similar length (≈1.50 μm) for 80 days. The immersion depth for all samples was 10 mm. Error bars were obtained from at least three independent measurements.

### *2.5.2. Anti-Fouling Mechanism and Superhydrophobicity Duration on Submerged NWs*

To confirm that fouling was completely suppressed on superhydrophobic NWs before wetting occurs, the absence of any settled marine species on the solid surfaces was confirmed by fluorescent microscopy. All surface geometries were immersed in the marine algae culture solution for 5 days and then dyed with LIVE/DEAD cell fluorescent dyes. As shown in Figures S14 and S16, Supporting Information, NWs in the Cassie–Baxter state showed no fluorescent signal, as there were no cells attached to the surface. However, the samples that were initially superhydrophobic eventually became wetted by the marine environment and collapsed into the Wenzel state. At this point, fouling initiated.

Since the transition from the Cassie–Baxter state to the Wenzel state drove the onset of fouling, the underwater duration of superhydrophobicity (i.e., the time for which the air layer remained "trapped" within the NW texture) is critical in determining the longevity of fouling prevention. In general, the underwater duration of superhydrophobicity depends on the total volume of the air layer, the applied hydrostatic pressure, and follows Fick's law of mass transfer at the air–water interface.[28] Specifically, the underwater duration of the air layer within the NW texture can be expressed as

$$\tau \approx V \cdot p^n \tag{1}$$

where $\tau$ is the duration of the air layer, $V$ is the total volume of the air layer, $p$ is the hydrostatic pressure, and $n$ is a constant depending on water properties (e.g., surface tension, oxygen, nitrogen level, etc.) and any present contaminants (e.g., biological species, ionic concentration, organic contaminants, etc.) (further details can be found in the Supporting Information).

Furthermore, water is known to vaporize at a different rate along curved air–water interfaces due to an increase in the Laplace pressure. Quantitatively, this change in vapor pressure is typically described by the Kelvin relation. This additional evaporation along a curved interface can be used to increase the stability of the gas layer when the surface pores are below a critical length (typically ≈ 1 μm).[29] Thus, to enhance the longevity of the superhydrophobic surfaces underwater,

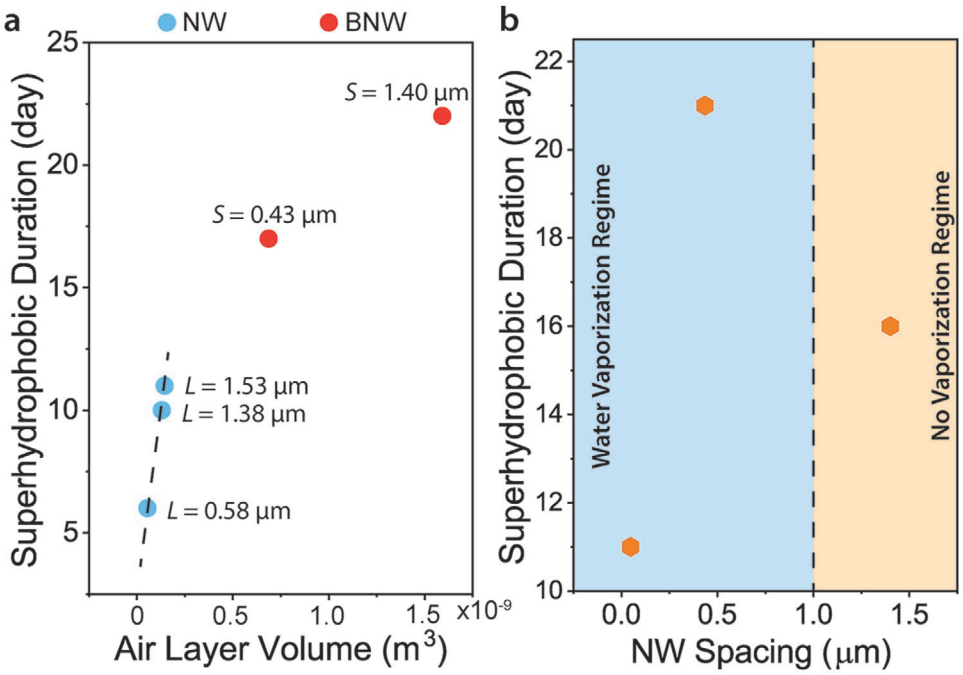


**Figure 8.** Superhydrophobic duration for NWs in the Cassie–Baxter state. a) Superhydrophobicity duration of NW surfaces with different length and degrees of hierarchy under marine algae fouling conditions. b) Superhydrophobic duration of NW surfaces with different spacing under the marine algae fouling conditions.

superhydrophobic NWs with a larger air volume and a spacing below 1 μm are desired.

From **Figure 8**a and Figure S18, Supporting Information, the superhydrophobic duration under the marine algae environment increased with the increase of the air layer volume on NWs with different length and degrees of hierarchy. Specifically, when the inter-NW spacing is fixed, the superhydrophobic duration on these surfaces increases linearly with the total volume of the air layer. In addition, the superhydrophobic duration increased with an increase in inter-NW spacing, when the spacing was less than the critical length (≈1 μm) (Figure 8a).[29] This is because the air layer volume increases with increasing inter-NW spacing, and all NWs with a spacing below 1 μm experience an enhancement in the superhydrophobicity duration as a result of the enhanced water vaporization. The vaporized water can partially replenish the air layer volume within submerged air-pockets, and thereby increase the lifetime.

In contrast, when the spacing of the NWs is larger than the critical length, the superhydrophobic duration decreases (Figure 8a). Interestingly, when the BNW architectures had a spacing between the base NWs of ≈1.40 μm (larger than the critical length), the superhydrophobic duration still increased. We attribute this to the fact that the spacing between the NW branches remained less than 1 μm, and thus the overall NW architecture possessed air pockets that can be stabilized by vaporized water. This demonstrates the utility provided by the control of hierarchical geometry at the nanoscale to tune the coupled wetting and fouling properties of superhydrophobic surfaces, and elucidates a set of design guidelines for nanostructured anti-fouling surfaces.

## 3. Conclusion

In this study, we fabricated optically transparent nanostructured surfaces with controlled geometric parameters, and systematically studied their structure–property relationships with respect to marine fouling. As part of our work, we fabricated NW surfaces with tunable control over their length, inter-NW spacing, and degrees of hierarchy spanning the nano-to-microscales.

For hydrophilic NWs, we demonstrated fouling reduction by up to 60% after 20 days, and a time-delay of 20 days before 100% fouling coverage. These anti-fouling properties were attributed to both size-selective settlement behavior and mechanical biocidal effects. For superhydrophobic NWs, we demonstrated that the non-fouling state can be maintained for up to 22 days and fouling can be delayed by more than 50 days.

By quantifying the coupled relationships between NW geometry, surface wettability, optical transparency, and interaction with marine algae, we have identified design guidelines that are supported by thermodynamic and mass transfer principles. Specifically, for hydrophilic NWs, the rate of fouling monotonically decreases with inter-NW spacing down to 50 nm, which is attributed to a combination of 1) size-selective settlement of marine species; and 2) a mechanical biocidal effect that arises from interactions at the NW tips. For superhydrophobic NWs, fouling can be completely suppressed when the unwetted Cassie–Baxter state is maintained, and can be delayed when the NWs transit to the wetted Wenzel state due to the same reasons described for hydrophilic NWs. The duration of underwater superhydrophobicity can be enhanced by increasing the volume of the air layer (through increasing NW length and introducing hierarchical branching) and optimizing inter-NW

spacing. In the future, the geometric design principles and mechanistic insights provided in this study could be applied to other nanostructured material systems, including durable polymer surfaces.[30] These insights can be used to rationally design nanostructured surfaces with anti-fouling properties for a broad range of applications, including marine fouling, biomedical devices, and the food industry.

## 4. Experimental Section

*Atomic Layer Deposition*: ZnO was deposited at a substrate temperature of 150 °C using diethyl zinc (DEZ) and DI water as the precursors. The ZnO was deposited as a polycrystalline film with a growth rate of ≈2.0 Å per cycle. $TiO_2$ was deposited at a substrate temperature of 175 °C using tetrakis(dimethylamido)titanium (TDMAT) and DI water as the precursors. The $TiO_2$ growth rate was measured to be ≈0.6 Å per cycle using ellipsometry. $Al_2O_3$ was deposited at a substrate temperature of 150 °C using trimethylaluminum (TMA) and DI water as the precursors. The $Al_2O_3$ growth rate was measured to be ≈1.0 Å per cycle using ellipsometry.

*ZnO NW Fabrication*: The ZnO NWs were grown in a solution using the sample concentration from our previous report.[15a] The hydrothermal growth was performed at 90 °C and ambient pressure. The substrates with ALD seed layers were suspended facing downward with angle ≈45° in the solution to prevent the homogeneous precipitate from settling on the surface. The total time for NW growth varied from 15 to 105 min after the solution temperature reached 90 °C. To avoid overheating the solution, the solution was gradually heated from room temperature (20 °C) to the reaction temperature (90 °C) at a rate of ≈1 °C $min^{-1}$. Therefore, the total submerged time for the samples varied between 75 and 165 min.

*Surface Chemistry Modification*: Heptadecafluoro-1,1,2,2-tetrahydrodecyltrichlorosilane (F-17) purchased from Gelest, Inc., was used to silanize the core–shell $ZnO/Al_2O_3$ NWs with different lengths, inter-NW spacings, and levels of branching to achieve superhydrophobicity. Thirty cycles of ALD $Al_2O_3$ (≈5 nm) was deposited on the NW surface as a buffer to provide reactive sites for silanization. The samples were cleaned in oxygen plasma for 10 min and maintained in a silane vapor environment at 120 °C for more than 3 h. After silanization process, the samples were rinsed with toluene to remove unbonded silane. The perfluorinated silane used to render the NWs to be superhydrophobic was chosen as an example surface functionalization to explore the geometric design principles for underwater superhydrophobic surfaces. Other alternative biocompatible surface modifications can also be applied to make NWs superhydrophobic, for example, the grafting of polydimethylsiloxane (PDMS) chains.[31]

*Contact Angle Measurements*: Contact angle measurements were performed with a Ramé-Hart 200-F1 contact angle goniometer using the sessile drop method. DI water and hexadecane (purchased from Thermo Fisher Scientific) were used as probe liquids. Advancing and receding contact angles were obtained by measuring the angle while the liquid was slowly added to or removed from a ≈3 µL droplet in contact with the sample and a micrometer syringe. At least five measurements were performed per sample, and the standard error is ±0.1°.

*Algal Fouling Experiments*: Marine green algae were raised in a fish tank at 25 °C with a standard bubbler and lighting for half-day on as a reservoir for algae biofilms. A total of 40% of the total volume was replaced with fresh culture solution every week. One gram of biomass (i.e., algae biofilm) was weighted through an analytical balance with a resolution of 0.0001 g and was introduced to a medium-sized petri dish (diameter: 100 mm) with 50 mL of seawater and F/2 (purchased from https://www.amazon.com/) mixture. Samples were cut into the same size (25 mm × 15 mm) before fabrication and submerged into the algae culture environment after being coated with different NWs. The bench culture in petri dishes was kept in room temperature (20 °C) with a lighting for half-day on. A total of 40% of the total volume (20 mL) was replaced in each petri dish culture with fresh culture solution every 5 days. The hydrostatic pressure on the testing samples was kept at ≈100 Pa.

*Algae Coverage Area Fraction Measurement*: The area fraction was quantified with microscopic images on the samples through ImageJ analysis. The microscopic images were taken over at least three different locations on each of the sample surfaces. The images were converted to 8 bit gray images and analyzed using ImageJ to obtain area coverage fraction. The Supporting Information shows three microscopic images (Figure S10a, Supporting Information) at different measurement spots on the hydrophilic NW sample after 20 days of fouling. In addition, Figure S10b, Supporting Information, shows the ImageJ analysis process on one of the microscopic images.

*Optical Density Measurements*: All samples were submerged in the algae culture solution for 20 days and rinsed by saltwater (0.8 M NaCl) to remove unattached algae. Then the samples were submerged in DMSO (Sigma-Aldrich) for 15 min to remove the chlorophyll in the algae, which would interfere in the signal of the trypan blue. After removing the chlorophyll, the samples were gently rinsed by saltwater again and stained with trypan blue (from Thermo Fisher Scientific) for 15 min, followed by rinsing off the excess dye. Finally, 10 mL of DMSO was used for each sample to extract the blue dye and absorbance of the liquid was measured by UV–vis spectrometry.

*Fluorescent Microscope Imaging*: The samples were all submerged in the algal culture solution for 5 days, and then were taken out and placed in sodium chloride (NaCl) solution (0.85%) with gentle stirring for 15 min to remove the unsettled algae. A LIVE/DEAD BacLight bacteria dye kit (Thermo Fisher Scientific L7012) was used to stain the fouled samples. The mixing ratio of LIVE/DEAD dye was 1:1, and the mixing ratio of dye to solution was 3 µL of dye to 1 mL of 0.85% NaCl. The samples were all stained with the dye solution for 15 min in dark environment. Fluorescent microscope images of each sample were taken through spinning disk confocal microscope (Olympus IX2-ZDC2) under the light with a wavelength of 480/500 nm (green) for total cells and 490/635 nm (red) for dead cells.

*ICP-MS Measurements*: A Zn ion calibration solution was prepared with concentrations of 5, 10, and 20 ppb. The measured concentration matched well with calibrated concentration and fitted linearly with $R^2 > 0.999$. The NW samples, with protection $Al_2O_3$ ALD overcoats in ≈5 and ≈15 nm, were submerged into 2 mL of DI water for 5 days. The fouling testing environment for each sample was 50 mL.

## Supporting Information

Supporting Information is available from the Wiley Online Library or from the author.

## Acknowledgements

This work was supported by DARPA Young Faculty Award D18AP00066. Any opinions, findings, conclusions, or recommendations expressed in this publication are those of the authors and do not necessarily reflect the views of DARPA. This material was based upon work supported by the National Science Foundation under grant no. 1751590. The authors thank Dr. James W. Gose at the Aaron Friedman Marine Hydrodynamics Laboratory of the University of Michigan for providing the marine algae, Jacob Hoffman for assistance with the algae fouling experiments, Maxwell S. DeNies and Prof. Allen P. Liu in Mechanical Engineering in the University of Michigan for assistance with fluorescent microscopic imaging, and Tae Cho and Dr. Eric Kazyak for assistance with electron microscopy imaging.

## Conflict of Interest

The authors have filed a provisional U.S. patent application related to this work.

## Keywords

atomic layer deposition, marine fouling, superhydrophobic nanowires, wetting

Received: April 17, 2020
Revised: June 4, 2020
Published online: July 26, 2020

[1] J. A. Callow, M. E. Callow, *Nat. Commun.* **2011**, *2*, 244.
[2] M. Schultz, J. Walker, C. Steppe, K. Flack, *Biofouling* **2015**, *31*, 759.
[3] H. A. Videla, L. K. Herrera, *Int. Microbiol.* **2005**, *8*, 169.
[4] L. Delauney, C. Compere, M. Lehaitre, *Ocean Sci.* **2010**, *6*, 503.
[5] D. V. Manov, G. C. Chang, T. D. Dickey, *J. Atmos. Oceanic Technol.* **2004**, *21*, 958.
[6] J. F. Schumacher, C. J. Long, M. E. Callow, J. A. Finlay, J. A. Callow, A. B. Brennan, *Langmuir* **2008**, *24*, 4931.
[7] G. Greco, T. S. Lanero, S. Torrassa, R. Young, M. Vassalli, A. Cavaliere, R. Rolandi, E. Pelucchi, M. Faimali, J. Davenport, *J. R. Soc., Interface* **2013**, *10*, 20130122.
[8] A. Scardino, D. Hudleston, Z. Peng, N. A. Paul, R. De Nys, *Biofouling* **2009**, *25*, 83.
[9] A. J. Scardino, R. de Nys, *Biofouling* **2011**, *27*, 73.
[10] a) M. Vucko, A. Poole, C. Carl, B. Sexton, F. Glenn, S. Whalan, R. De Nys, *Biofouling* **2014**, *30*, 1; b) J. F. Schumacher, N. Aldred, M. E. Callow, J. A. Finlay, J. A. Callow, A. S. Clare, A. B. Brennan, *Biofouling* **2007**, *23*, 307; c) A. V. Bers, M. Wahl, *Biofouling* **2004**, *20*, 43; d) J. F. Schumacher, M. L. Carman, T. G. Estes, A. W. Feinberg, L. H. Wilson, M. E. Callow, J. A. Callow, J. A. Finlay, A. B. Brennan, *Biofouling* **2007**, *23*, 55; e) M. L. Carman, T. G. Estes, A. W. Feinberg, J. F. Schumacher, W. Wilkerson, L. H. Wilson, M. E. Callow, J. A. Callow, A. B. Brennan, *Biofouling* **2006**, *22*, 11.
[11] a) E. P. Ivanova, J. Hasan, H. K. Webb, G. Gervinskas, S. Juodkazis, V. K. Truong, A. H. F. Wu, R. N. Lamb, V. A. Baulin, G. S. Watson, J. A. Watson, D. E. Mainwaring, R. J. Crawford, *Nat. Commun.* **2013**, *4*, 2838; b) D. P. Linklater, M. De Volder, V. A. Baulin, M. Werner, S. Jessl, M. Golozar, L. Maggini, S. Rubanov, E. Hanssen, S. Juodkazis, *ACS Nano* **2018**, *12*, 6657; c) S. Pogodin, J. Hasan, V. A. Baulin, H. K. Webb, V. K. Truong, T. H. P. Nguyen, V. Boshkovikj, C. J. Fluke, G. S. Watson, J. A. Watson, *Biophys. J.* **2013**, *104*, 835; d) E. P. Ivanova, J. Hasan, H. K. Webb, V. K. Truong, G. S. Watson, J. A. Watson, V. A. Baulin, S. Pogodin, J. Y. Wang, M. J. Tobin, *Small* **2012**, *8*, 2489; e) S.-H. Hong, J. Hwang, H. Lee, *Nanotechnology* **2009**, *20*, 385303; f) S. Pandit, K. Gaska, V. R. Mokkapati, E. Celauro, A. Derouiche, S. Forsberg, M. Svensson, R. Kádár, I. Mijakovic, *Small* **2020**, *16*, 1904756; g) J. Jenkins, J. Mantell, C. Neal, A. Gholinia, P. Verkade, A. H. Nobbs, B. Su, *Nat. Commun.* **2020**, *11*, 1626; h) S. G. Higgins, M. Becce, A. Belessiotis-Richards, H. Seong, J. E. Sero, M. M. Stevens, *Adv. Mater.* **2020**, *32*, 1903862; i) N. P. Dasgupta, J. Sun, C. Liu, S. Brittman, J. Lim, H. Gao, R. Yan, P. Yang, *Adv. Mater.* **2014**, *26*, 2137.
[12] a) M. Wahl, *Mar. Ecol.: Prog. Ser.* **1989**, *58*, 175; b) D. M. Yebra, S. Kiil, K. Dam-Johansen, *Prog. Org. Coat.* **2004**, *50*, 75; c) L. D. Chambers, K. R. Stokes, F. C. Walsh, R. J. Wood, *Surf. Coat. Technol.* **2006**, *201*, 3642; d) C. M. Magin, S. P. Cooper, A. B. Brennan, *Mater. Today* **2010**, *13*, 36.
[13] a) T. L. Liu, C.-J. C. Kim, *Science* **2014**, *346*, 1096; b) H. J. Fan, P. Werner, M. Zacharias, *Small* **2006**, *2*, 700; c) C. Vieu, F. Carcenac, A. Pepin, Y. Chen, M. Mejias, A. Lebib, L. Manin-Ferlazzo, L. Couraud, H. Launois, *Appl. Surf. Sci.* **2000**, *164*, 111.
[14] a) M. P. Stoykovich, M. Müller, S. O. Kim, H. H. Solak, E. W. Edwards, J. J. De Pablo, P. F. Nealey, *Science* **2005**, *308*, 1442; b) O. Ikkala, G. ten Brinke, *Science* **2002**, *295*, 2407; c) S. Mann, *Nat. Mater.* **2009**, *8*, 781.
[15] a) A. R. Bielinski, M. Boban, Y. He, E. Kazyak, D. H. Lee, C. Wang, A. Tuteja, N. P. Dasgupta, *ACS Nano* **2017**, *11*, 478; b) A. R. Bielinski, E. Kazyak, C. M. Schlepütz, H. J. Jung, K. N. Wood, N. P. Dasgupta, *Chem. Mater.* **2015**, *27*, 4799.
[16] Y. Chen, N. J. Ginga, W. S. LePage, E. Kazyak, A. J. Gayle, J. Wang, R. E. Rodríguez, M. D. Thouless, N. P. Dasgupta, *ACS Appl. Mater. Interfaces* **2019**, *11*, 43573.
[17] R. N. Wenzel, *Ind. Eng. Chem.* **1936**, *28*, 988.
[18] a) A. Lafuma, D. Quéré, *Nat. Mater.* **2003**, *2*, 457; b) A. Checco, B. M. Ocko, A. Rahman, C. T. Black, M. Tasinkevych, A. Giacomello, S. Dietrich, *Phys. Rev. Lett.* **2014**, *112*, 216101.
[19] W. Choi, A. Tuteja, J. M. Mabry, R. E. Cohen, G. H. McKinley, *J. Colloid Interface Sci.* **2009**, *339*, 208.
[20] J. Monty, E. Dogan, R. Hanson, A. Scardino, B. Ganapathisubramani, N. Hutchins, *Biofouling* **2016**, *32*, 451.
[21] a) K. Z. Hunsucker, A. Koka, G. Lund, G. Swain, *Biofouling* **2014**, *30*, 1133; b) S. V. Dobretsov, P.-Y. Qian, *Biofouling* **2002**, *18*, 217.
[22] G. B. Hwang, K. Page, A. Patir, S. P. Nair, E. Allan, I. P. Parkin, *ACS Nano* **2018**, *12*, 6050.
[23] a) T. Diu, N. Faruqui, T. Sjöström, B. Lamarre, H. F. Jenkinson, B. Su, M. G. Ryadnov, *Sci. Rep.* **2015**, *4*, 7122; b) Y. Q. Li, B. Zhu, Y. Li, W. R. Leow, R. Goh, B. Ma, E. Fong, M. Tang, X. Chen, *Angew. Chem., Int. Ed.* **2014**, *53*, 5837.
[24] Y. Song, U. Kadiyala, P. Weerappuli, J. J. Valdez, S. Yalavarthi, C. Louttit, J. S. Knight, J. J. Moon, D. S. Weiss, J. S. VanEpps, *Adv. Mater.* **2019**, *31*, 1807436.
[25] F. Wu, B. J. Harper, S. L. Harper, *Environ. Toxicol. Chem.* **2019**, *38*, 591.
[26] W. Hu, C. Peng, W. Luo, M. Lv, X. Li, D. Li, Q. Huang, C. Fan, *ACS Nano* **2010**, *4*, 4317.
[27] Y. Tu, M. Lv, P. Xiu, T. Huynh, M. Zhang, M. Castelli, Z. Liu, Q. Huang, C. Fan, H. Fang, *Nat. Nanotechnol.* **2013**, *8*, 594.
[28] a) K. Holmén, P. Liss, *Tellus B* **1984**, *36*, 92; b) R. Poetes, K. Holtzmann, K. Franze, U. Steiner, *Phys. Rev. Lett.* **2010**, *105*, 166104.
[29] P. R. Jones, X. Hao, E. R. Cruz-Chu, K. Rykaczewski, K. Nandy, T. M. Schutzius, K. K. Varanasi, C. M. Megaridis, J. H. Walther, P. Koumoutsakos, *Sci. Rep.* **2015**, *5*, 12311.
[30] K. Golovin, M. Boban, J. M. Mabry, A. Tuteja, *ACS Appl. Mater. Interfaces* **2017**, *9*, 11212.
[31] a) L. Wang, T. J. McCarthy, *Angew. Chem., Int. Ed.* **2016**, *55*, 244; b) J. Wang, L. Wang, N. Sun, R. Tierney, H. Li, M. Corsetti, L. Williams, P. K. Wong, T.-S. Wong, *Nat. Sustainability* **2019**, *2*, 1097; c) L. Zhang, Z. Guo, J. Sarma, X. Dai, *ACS Appl. Mater. Interfaces* **2020**, *12*, 20084.

 